Reg # 12639

[redacted]

Copy 221
RM L54G13

NACA RM L54G13

TECH LIBRARY KAFB, NM
0144145

7563

NACA

RESEARCH MEMORANDUM

SOME EFFECTS OF AILERON SPAN, AILERON CHORD, AND WING TWIST ON ROLLING EFFECTIVENESS AS DETERMINED BY ROCKET-POWERED MODEL TESTS AND THEORETICAL ESTIMATES

By H. Kurt Strass and Warren A. Tucker

Langley Aeronautical Laboratory
Langley Field, Va.

[redacted]

NATIONAL ADVISORY COMMITTEE
FOR AERONAUTICS
WASHINGTON
September 14, 1954

[redacted]

[redacted]

TECH LIBRARY KAFB, NM
0144145

 [redacted]

NATIONAL ADVISORY COMMITTEE FOR AERONAUTICS

RESEARCH MEMORANDUM

SOME EFFECTS OF AILERON SPAN, AILERON CHORD, AND WING TWIST ON ROLLING EFFECTIVENESS AS DETERMINED BY ROCKET-POWERED MODEL TESTS AND THEORETICAL ESTIMATES

By H. Kurt Strass and Warren A. Tucker

SUMMARY

The variation of rolling effectiveness with spanwise aileron extent has been determined for full-chord ailerons on a sweptback wing over a Mach number range of approximately 0.5 to 1.5 by the Langley Pilotless Aircraft Research Division utilizing rocket-propelled test vehicles in free flight. The test wings had NACA 65A006 airfoil sections, an aspect ratio of 4.0, 45° sweepback at the quarter-chord line, and a taper ratio of 0.6. These data were correlated with the results of a similar investigation concerning partial-chord ailerons. This correlation shows that the spanwise variation of aileron effectiveness for an aileron of given chord exhibited little variation with Mach number over a range of 0.6 to 1.4, and also shows that 0.3-chord ailerons were relatively less effective near the wing tip than either full-chord or 0.15-chord ailerons. In addition, tests were made by using models with twisted wings to provide a limited check upon the principle of aerodynamic superposition.

Values of rolling effectiveness calculated for the full-chord ailerons and the twisted wings by means of linear theory agreed well with the experimental data.

INTRODUCTION

A general investigation of wing-control rolling effectiveness is being conducted by the Langley Pilotless Aircraft Research Division utilizing rocket-propelled test vehicles in free flight at transonic and supersonic speeds. In continuance of this program, the variation of rolling effectiveness with spanwise aileron extent was obtained for full-chord ailerons and these data were correlated with the results of a

[redacted]

[redacted]

previous similar investigation concerning partial-chord trailing-edge ailerons (ref. 1) to show some effects of aileron chord.

The principle of aerodynamic superposition is frequently used in calculating the effects of aeroelasticity by assuming that the characteristics of the twisted wing can be obtained by superposing the results of calculations made for unit deflection of partial-span segments (see appendix). A limited check upon this principle was made by comparing the results of the full-chord aileron with data obtained from flight test models which employed twisted wings. In addition, calculated values for all the test configurations are presented.

SYMBOLS

A aspect ratio, b^2/S

b diameter of circle swept by wing tips, ft

c wing chord measured parallel to model center line, ft

c_a aileron chord, ft

c_r wing root chord, ft

$K_1 = \frac{1 - \lambda}{1 - k}$

$K_2 = \beta m K_1$

$K_3 = (1 + \beta m)K_1$

$k = \frac{\text{Cotangent of leading-edge sweepback}}{\text{Cotangent of trailing-edge sweepback}}$

L rolling moment (positive when tending to depress right wing, as seen from rear), ft-lb

n section normal force

M Mach number

T twisting couple applied at wing tip in a plane perpendicular to the wing chord plane and parallel to the model center line, in-lb

m cotangent of leading-edge sweepback

p rolling velocity, radians/sec

q dynamic pressure, lb/sq ft

R Reynolds number based on mean exposed wing chord

S area of two wings taken to fuselage center line, sq ft

$\frac{pb}{2V}$ rolling effectiveness parameter (wing-tip helix angle), radians

V velocity, ft/sec

$C_l = \frac{L}{qSb}$

C_{l_δ} rolling-moment effectiveness for two ailerons $\left(\frac{\partial C_l}{\partial \delta}\right)_{\delta \to 0}$

$(C_{l_\delta})_f$ value of C_{l_δ} for full-chord-aileron configuration when used in superposition equation

C_{l_p} damping-in-roll derivative $\left(\frac{\partial C_l}{\partial \frac{pb}{2V}}\right)_{\frac{pb}{2V} \to 0}$

C_p pressure coefficient, $\frac{\text{Pressure difference between upper and lower surfaces}}{q}$

I_n value of integral in region n (see eq. (A3))

K_{η_i} $\frac{\left(\frac{pb}{2V}\right)_{\text{partial span}} / \delta_a}{\left(\frac{pb}{2V}\right)_{\text{full exposed span}} / \delta_a}$

α local angle of incidence of twisted wing

$\beta = \sqrt{M^2 - 1}$

δ_a average aileron deflection measured in a plane perpendicular to chord plane and parallel to model center line, average of three wings, deg

δ_t average tip angle of incidence of twisted wing, deg

[redacted]

[redacted]

Λ angle of sweep measured at $c/4$, deg

λ ratio of tip chord to extended chord at model center line

ξ,η rectangular coordinates, normalized with respect to wing root chord and wing semispan, respectively

η_i value of η at inboard end of aileron

θ twist of wing measured in a plane perpendicular to the wing-chord plane and parallel to the model center line, radians

MODELS AND TECHNIQUE

The general arrangement including some significant physical dimensions of the test vehicles used in this investigation is presented in figures 1 and 2. Some typical details of the test models are shown in the photographs presented as figure 3. The outer portions of the wings on models 1 to 4 were rotated about the 40-percent-chord line (see fig. 3(c)). No attempt was made to seal the gap thus created. The spanwise locations of the inboard ends of the full-chord ailerons are given in table I in conjunction with other significant information. The aileron deflections of models 1 to 4 were increased as the spanwise extent was decreased (see table I), thus maintaining sufficient rolling effectiveness to insure good experimental accuracy.

For reference, figure 4 presents a comparison of the spanwise variation of the torsional stiffness parameter $\frac{\theta}{T}$ for all of the test models.

Models 5, 6, and 7 employed twisted wings wherein the angle of incidence was proportional to the cube of the distance from the fuselage center line ($\alpha = \delta_t\eta^3$). Model 5 was constructed with 4.5-percent-thick wings which were made by scaling down the ordinates of the NACA 65A006 airfoil section.

The flight tests were made at the Langley Pilotless Aircraft Research Station at Wallops Island, Va. The test vehicles were propelled to supersonic speeds by a two-stage rocket-propulsion system. During a period of approximately 12 seconds of coasting flight following rocket-motor burnout, time histories of the rolling velocity were obtained with special radio equipment (spinsonde) and the flight-path velocity was obtained by use of CW Doppler radar. These data, in conjunction with atmospheric data obtained with radiosondes, permit the evaluation of the control rolling effectiveness in terms of the parameter $pb/2V$ as a function of Mach number.

Figure 5 presents the average variation of Reynolds number with Mach number for the models discussed in this paper.

ACCURACY

From previous experience and mathematical analysis it is estimated that the maximum experimental error is within the following limits:

	Subsonic	Supersonic
$\frac{pb/2V}{\delta}$, radians	$\pm\frac{0.003}{\delta}$	$\pm\frac{0.002}{\delta}$
M	±0.01	±0.005

where δ is either δ_a or δ_t.

DATA CORRECTIONS AND REDUCTION

All of the data have been reduced to $\frac{pb/2V}{\delta}$ in order to allow direct comparison of the various wing modifications. No attempt was made to correct for the effects of test-vehicle moment of inertia about the roll axis on the measured variation of $pb/2V$ with Mach number since previous experience has demonstrated that the effects are within the accuracy of measurement.

The data are presented two ways:

1. Uncorrected for the effects of aeroelasticity

2. Corrected to estimated rigid wing values

The rigid wing estimates were made by the method given in reference 2 by using span load distributions obtained from reference 3 and wind-tunnel data.

RESULTS AND DISCUSSION

Ailerons

Figure 6 presents the variation of the rolling effectiveness parameter $\frac{pb}{2V}\Big/\delta_a$ with Mach number for the models employing full-chord

[redacted]

ailerons. These data are compared with values calculated by linear theory as described in the appendix and by strip theory. The agreement between corrected experiment and linear theory is excellent except for the supersonic values for model 1. A contributing factor to this discrepancy may be the approximation of the actual three-wing model by a two-wing configuration for calculation purposes, and an additional factor may be the neglect of the effect of the body (see appendix); both these factors are relatively more important for model 1 than for the other models.

Reference 4 presents a simplified method for estimating the rolling effectiveness of all-movable wings (full-exposed-span full-chord ailerons). This method (strip theory) was applied also to partial-span ailerons and the resulting estimates are also presented in figure 6. These results show that strip theory underestimates the full-exposed-span case (model 1) slightly and overestimates the extreme outboard (model 4) ailerons by a larger proportion.

The data of figure 6 are expressed as a fraction of the full-exposed-span rolling effectiveness and are cross-plotted in figure 7 to show the spanwise variation of rolling effectiveness with extent of aileron span. Envelope curves enclose the total scatter experienced in the Mach number range from $0.6 \leqq M \leqq 1.4$. In addition, comparison was made in a similar manner with the results of a similar investigation concerning partial-chord trailing-edge ailerons (ref. 1). For consistency with the present results, new rigid wing corrections were made for the partial-chord ailerons utilizing the method of reference 2. The spanwise variations thus obtained exhibited little variation with Mach number. For this reason, faired averaged curves were prepared. These curves are presented in figure 8 and are applicable over a Mach number range of $0.6 \leqq M \leqq 1.4$. This correlation which averages the effects of Mach number shows that the 0.3-chord ailerons were relatively less effective near the wing tip than either the full-chord or the 0.15-chord ailerons.

Twisted Wings

Figure 9 presents a comparison of the rolling effectiveness resulting from cubic distribution of wing twist with several methods of estimation. A limited check upon the validity of the principle of superposition when applied to experimental data is presented in the comparison of the data for models 5 and 6 with the value estimated from the cross plot of figure 8. This estimate was made in a manner similar to that used in the

appendix for the swept cubic-twist configurations. In this instance, the rolling effectiveness of the twisted wing can be expressed as follows:

$$\frac{pb}{2V} = \frac{\left(\frac{pb}{2V}\right)_{\text{full-exposed span}}}{\delta_a} \int_{\alpha\ \text{root}}^{\alpha\ \text{tip}} K_{\eta_i}\, d\alpha$$

where

$$\alpha = \delta_t \eta^3$$

then

$$\frac{pb/2V}{\delta_t} = 3\,\frac{\left(\frac{pb}{2V}\right)_{\text{full-exposed span}}}{\delta_a} \int_0^1 K_{\eta_i} \eta_i^2 d\eta_i$$

Models 5 and 6 agreed well when corrected for the effects of aeroelasticity thus indicating that the effects of wing thickness are small in this thickness range as might be expected. The experimental estimate should be equally good at speeds lower than $M = 0.6$ as Mach number effects in this range are negligible. Good agreement was also obtained from the linear and strip theory estimates. Little effect of wing sweepback is apparent as the results of the tests of the unswept wing (model 7) are in good agreement with the swept-wing results.

CONCLUDING REMARKS

A free-flight investigation employing rocket-powered test vehicles was made at Mach numbers ranging from 0.5 to 1.5 to determine the variation of rolling effectiveness with extent of aileron span employing full-chord ailerons on a wing of aspect ratio 4.0, sweepback 45°, taper ratio of 0.6, and employing NACA 65A006 airfoil sections. These data were correlated with the results of a similar investigation concerning partial-chord ailerons. This correlation shows that the spanwise variation of aileron effectiveness for an aileron of given chord exhibited little variation with Mach number over a range of 0.6 to 1.4, and also shows that 0.3-chord ailerons were relatively less effective near the wing tip than either full-chord or 0.15-chord ailerons.

Additional tests using models with twisted wings showed good agreement with estimates based upon the full-chord aileron tests thus providing a limited check upon the principle of aerodynamic superposition.

Agreement of the test results with estimates using linear theory was good.

Langley Aeronautical Laboratory,
National Advisory Committee for Aeronautics,
Langley Field, Va., June 24, 1954.

APPENDIX

THEORETICAL ESTIMATIONS

INTRODUCTION

Because of the variety of the configurations tested and the Mach number range covered, it was necessary to use several methods in calculating theoretical values of $pb/2V$. For all cases, the following relation was used:

$$\frac{pb/2V}{\delta} = \frac{C_{l_\delta}}{C_{l_p}} \tag{A1}$$

The calculations were carried out as if the models had two wing panels in one plane, rather than three equally spaced panels, and the presence of the body was neglected. Past experience with models similar to the present ones has shown that this procedure is an acceptable one for estimates of $pb/2V$. The various sources (refs. 3, 5 to 8) from which values of C_{l_δ} and C_{l_p} were obtained are listed in table II. In most instances, the required quantities could be obtained from the references cited directly enough to require no further explanation. However, some additional work was required in order to estimate values of C_{l_δ} at supersonic speeds for the full-chord-aileron and the swept cubic-twist configurations. This work is described in the following sections.

Full-Chord-Aileron Configurations

Briefly, the rolling moment for the full-chord-aileron configurations was found by determining the pressure in the various regions of the wing influenced by the aileron, integrating this pressure in the chordwise direction to obtain the span load distribution, and finally integrating the span load distribution to arrive at the rolling moment.

The axis system and rotation used in the calculations is shown in figure 10. The full-chord aileron, represented by the shaded area, is at an angle of incidence δ_a; the rest of the wing is at zero angle of incidence. The pressure in regions 1, 2, 3, and 4 is given by equation (6.4) of reference 9. In the notation of the present paper, the pressure coefficient is expressed as follows:

$$C_p = \frac{8\delta}{\beta\pi}\frac{K_2}{K_3}\sqrt{\frac{\xi + K_2\eta - K_3\eta_i}{\xi - K_1\eta}} \tag{A2}$$

The pressure in region 5 can be shown to be zero. Therefore the span load distribution is found by integrating equation (A2) with respect to ξ over each of the regions 1, 2, 3, and 4, using the limits appropriate to each region. Thus, if n is the section normal force, then the span load is given by the following equation:

$$\frac{n}{qc_r} = \frac{8\delta}{\beta\pi}\frac{K_2}{K_3}\int_{\text{lower limit}}^{\text{upper limit}}\sqrt{\frac{\xi + K_2\eta - K_3\eta_i}{\xi - K_1\eta}}\,d\xi = \frac{8\delta}{\beta\pi}\frac{K_2}{K_3}I_n \tag{A3}$$

where the upper and lower limits are those appropriate to the particular region as shown in figure 10, and I_n is the result of the integration, the subscript n corresponding to the number of the particular region. The expressions for I_n are as follows:

$$\left.\begin{aligned}
I_1 &= K_3\left[\sqrt{(1 - \eta_i)(1 - \eta)} + (\eta - \eta_i)\sinh^{-1}\sqrt{\frac{1 - \eta}{\eta - \eta_i}}\right] \\
I_2 &= \sqrt{\left[1 - K_1(1 - k)\eta + K_3(\eta - \eta_i)\right]\left[1 - K_1(1 - k)\eta\right]} + \\
&\qquad K_3(\eta - \eta_i)\sinh^{-1}\sqrt{\frac{1 - K_1(1 - k)\eta}{K_3(\eta - \eta_i)}} \\
I_3 &= \sqrt{\left[1 - K_1(1 - k)\eta - K_3(\eta_i - \eta)\right]\left[1 - K_1(1 - k)\eta\right]} - \\
&\qquad K_3(\eta_i - \eta)\cosh^{-1}\sqrt{\frac{1 - K_1(1 - k)\eta}{K_3(\eta_i - \eta)}} \\
I_4 &= \sqrt{\left[1 - K_1(1 + k)\eta - K_3(\eta_i - \eta)\right]\left[1 - K_1(1 + k)\eta\right]} - \\
&\qquad K_3(\eta_i - \eta)\cosh^{-1}\sqrt{\frac{1 - K_1(1 + k)\eta}{K_3(\eta_i - \eta)}}
\end{aligned}\right\} \tag{A4}$$

The calculations for $\eta_i = 0.918$ (model 4) required the consideration of an additional type of region, as shown in figure 11 (compare with

figure 10). The pressure is zero in regions 7 and 8, and the regions 1 and 3 are the same as those in figure 10. Region 6, however, has no counterpart in figure 10; the value of I_6 is as follows:

$$I_6 = K_3 \left[\sqrt{(1 - \eta_i)(1 - \eta)} - (\eta_i - \eta) \cosh^{-1}\sqrt{\frac{1 - \eta}{\eta_i - \eta}}\right] \tag{A5}$$

Plots of the quantity $\frac{8}{\pi}\frac{K_2}{K_3} I_n$ are presented in figure 12 for a value of $\beta m = 0.765$, for the values of η_i corresponding to the models tested.

After the span load has been obtained as just described, an additional integration with respect to η gives the value for C_{l_δ}. The final result has the following form:

$$C_{l_\delta} = \frac{8}{\pi\beta}\frac{K_2}{K_3}\frac{1}{1 + \lambda}\int_{-1}^{1} \eta I_n \, d\eta \tag{A6}$$

The integration was done graphically, using the values shown in figure 12. The span load for $\eta_i = 0.139$ is not correct for values of η less than -0.78 because the effect of the left wing tip was neglected; the error incurred can be shown to be less than 2 percent in the final C_{l_δ} value.

Swept Cubic-Twist Configurations

For the swept cubic-twist configurations (models 5 and 6) the value of the rolling moment was calculated by superposition of the preceding results for the full-chord-aileron configurations. If α is the angle of incidence at any spanwise station and $(C_{l_\delta})_f$ the corresponding value of C_{l_δ} for the full-chord-aileron configuration, then for an arbitrary distribution of angle of incidence the following equation applies:

$$C_l = \int_{\alpha_{root}}^{\alpha_{tip}} (C_{l_\delta})_f \, d\alpha \tag{A7}$$

For the particular case of the cubic-twist wing,

$$\alpha = \delta_t \eta^3 \tag{A8}$$

where δ_t is the tip angle of incidence, so that for this case

$$C_{l_\delta} = 3\int_0^1 (C_{l_\delta})_f \eta_i^2 d\eta_i \tag{A9}$$

The integration was performed graphically to arrive at the numerical values of C_{l_δ} for the swept cubic-twist configuration.

REFERENCES

1. Schult, Eugene D., Strass, H. Kurt, and Fields, E. M.: Free-Flight Measurements of Some Effects of Aileron Span, Chord, and Deflection and of Wing Flexibility of the Rolling Effectiveness of Ailerons on Sweptback Wings at Mach Numbers Between 0.8 and 1.6. NACA RM L51K16, 1952.

2. Strass, H. Kurt, and Stephens, Emily W.: An Engineering Method for the Determination of Aeroelastic Effects Upon the Rolling Effectiveness of Ailerons on Swept Wings. NACA RM L53H14, 1953.

3. DeYoung, John: Theoretical Antisymmetric Span Loading for Wings of Arbitrary Plan Form at Subsonic Speeds. NACA Rep. 1056, 1951. (Supersedes NACA TN 2140.)

4. Strass, H. Kurt, and Marley, Edward T.: Rolling Effectiveness of All-Movable Wings at Small Angles of Incidence at Mach Numbers From 0.6 to 1.6. NACA RM L51H03, 1951.

5. Alden, Henry L., and Schindel, Leon H.: The Lift, Rolling Moment, and Pitching Moment on Wings in Nonuniform Supersonic Flow. Jour. Aero. Sci., vol. 19, no. 1, Jan. 1952, pp. 7-14.

6. Martin, John C., and Jeffreys, Isabella: Span Load Distributions Resulting From Angle of Attack, Rolling, and Pitching for Tapered Sweptback Wings With Streamwise Tips - Supersonic Leading and Trailing Edges. NACA TN 2643, 1952.

7. Malvestuto, Frank S., Jr., Margolis, Kenneth, and Ribner, Herbert S.: Theoretical Lift and Damping in Roll at Supersonic Speeds of Thin Sweptback Tapered Wings With Streamwise Tips, Subsonic Leading Edges, and Supersonic Trailing Edges. NACA Rep. 970, 1950. (Supersedes NACA TN 1860.)

8. Harmon, Sidney M., and Jeffreys, Isabella: Theoretical Lift and Damping in Roll of Thin Wings With Arbitrary Sweep and Taper at Supersonic Speeds - Supersonic Leading and Trailing Edges. NACA TN 2114, 1950.

9. Lagerstrom, P. A.: Linearized Supersonic Theory of Conical Wings. NACA TN 1685 (Corrected copy), 1950.

TABLE I.- DESCRIPTION OF TEST MODELS

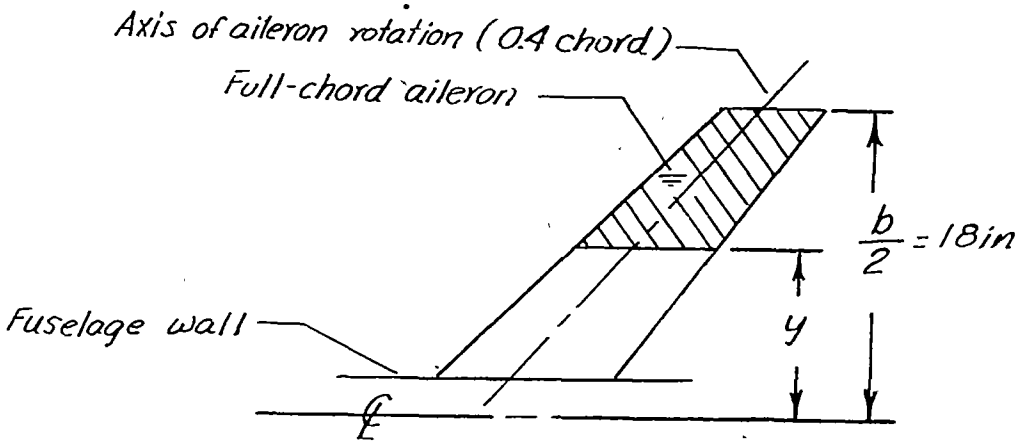

$$\eta_i = \frac{2y}{b}$$

Model	c/4, deg	η_i	δ_α, deg	δ_t, deg	NACA airfoil section
1	45	0.139	1.41	----	65A006
2	45	.487	1.63	----	65A006
3	45	.705	2.77	----	65A006
4	45	.918	4.75	----	65A006
5	45	.139	----	5.17	$65_{(06)}$A004.5
6	45	.139	----	4.82	65A006
7	0	.139	----	4.71	65A006

TABLE II.- REFERENCES FOR THEORETICAL ESTIMATES

Type of wing	Model	Subsonic	Supersonic	
		C_{l_δ} and C_{l_p}	C_{l_δ}	C_{l_p}
Full-chord aileron	1, 2, 3, 4	Reference 3	Present paper	Reference 7
Cubic twist (swept)	5, 6	Reference 3	Present paper	Reference 7
Cubic twist (unswept)	7	Reference 3	References 5 and 6	Reference 8

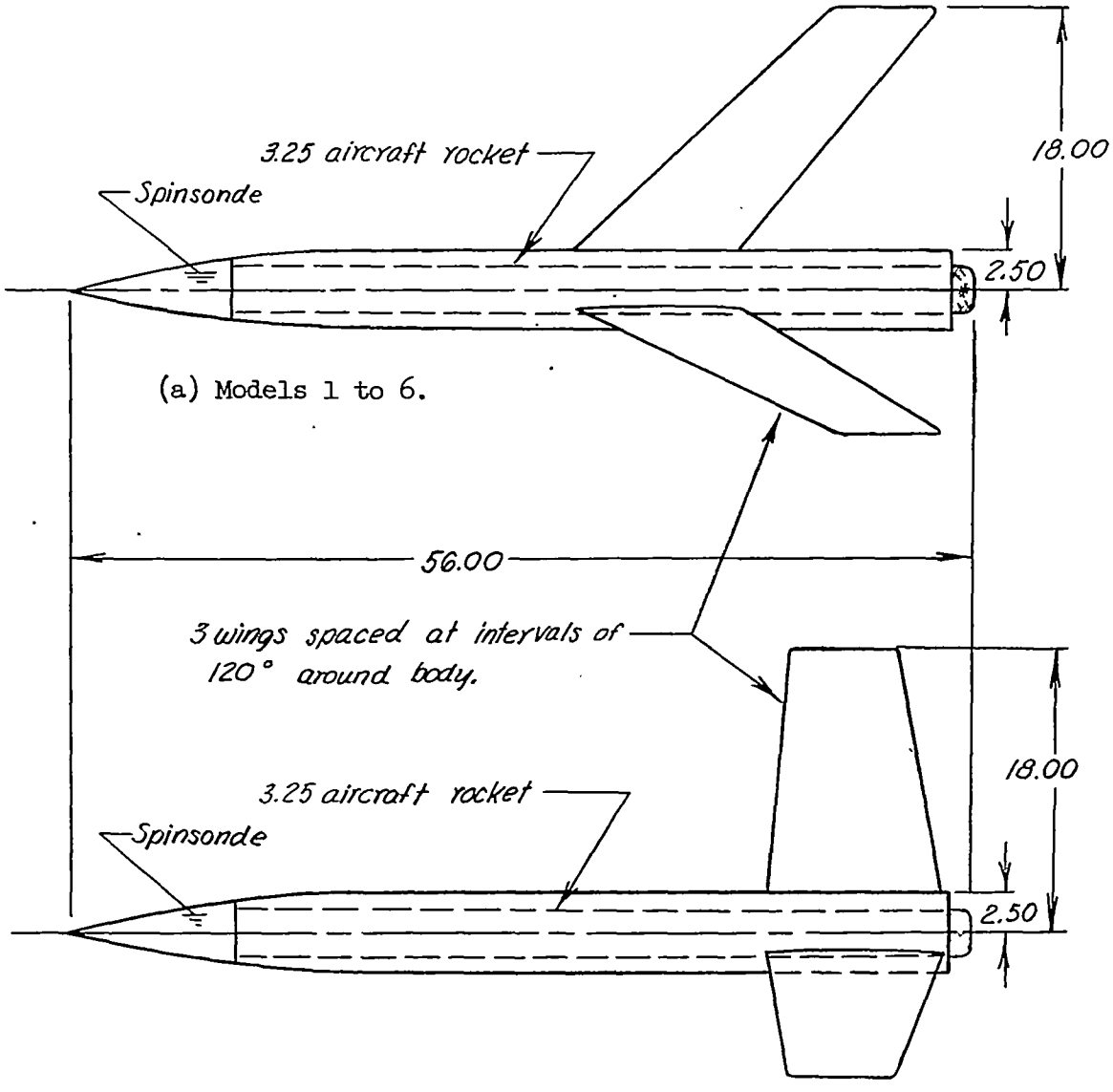

(b) Model 7.

Figure 1.- General arrangement of flight test vehicles. All dimensions are in inches.

[redacted]

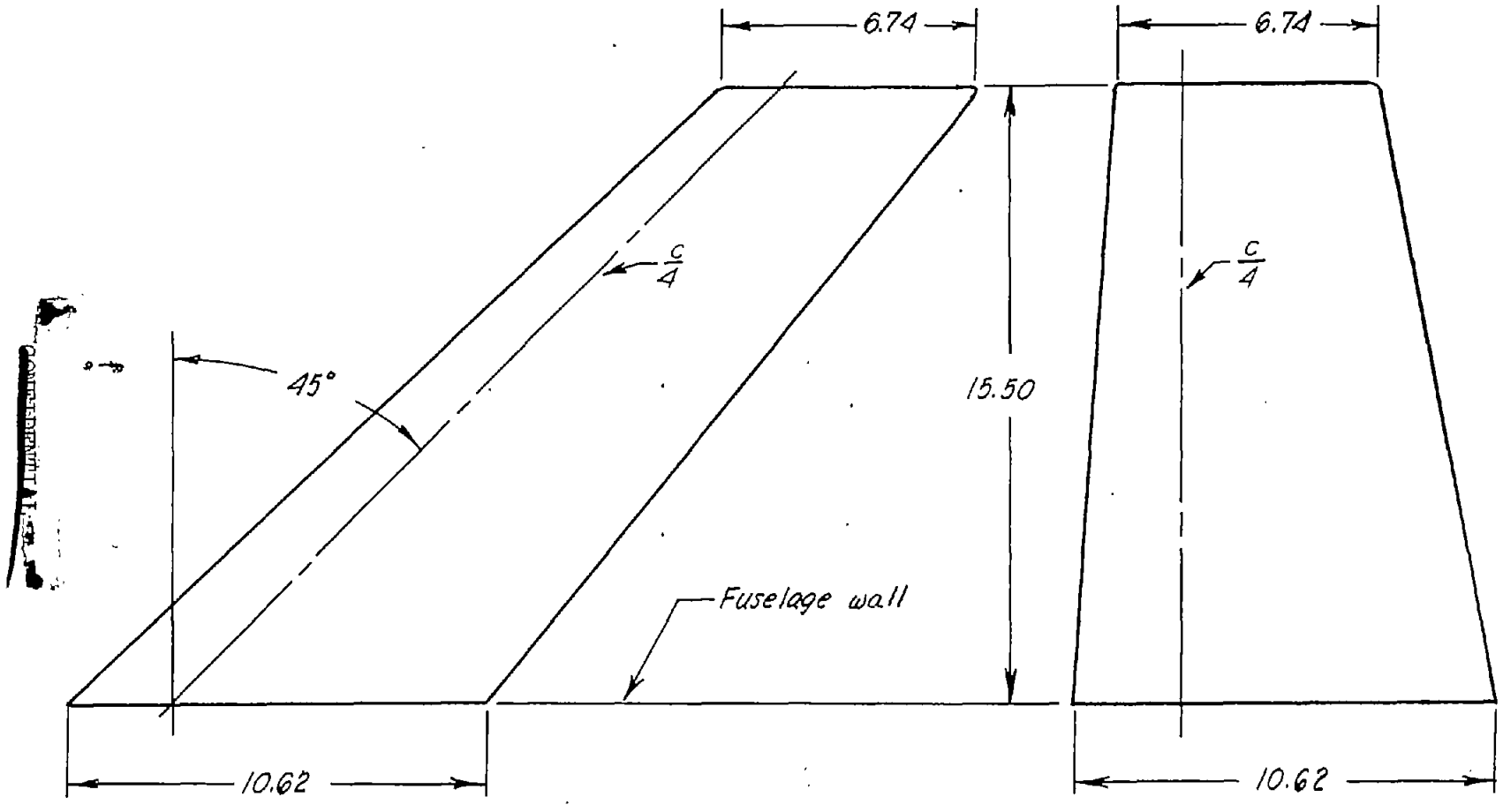

(a) Models 1 to 6. $\Lambda = 45^{\circ}$.

(b) Model 7. $\Lambda = 0^{\circ}$.

Figure 2.- Wing plan-form geometry of test vehicles. All dimensions are in inches.

CONFIDENTIAL

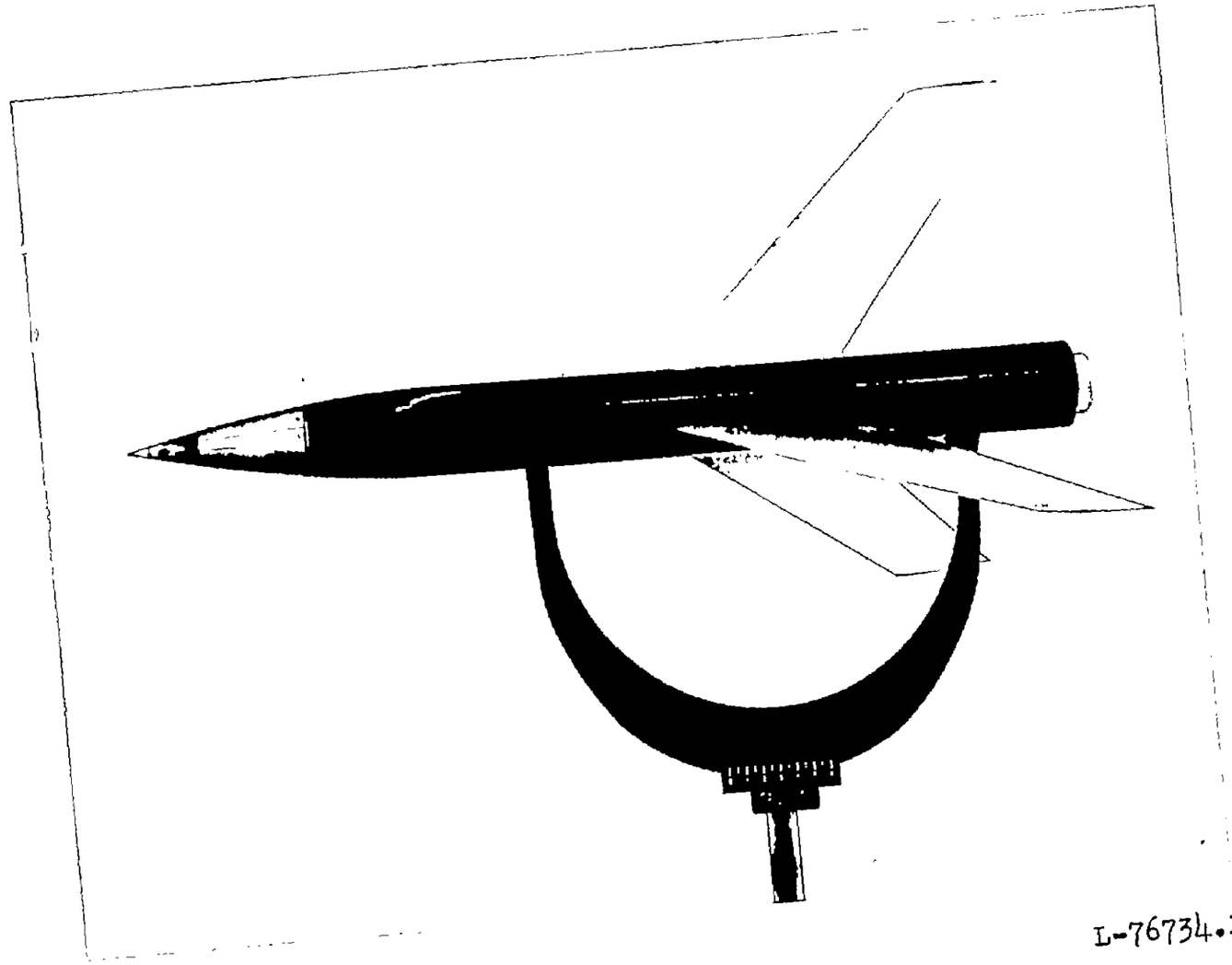

(a) General arrangement. Model 5.

Figure 3.- Photographs of test vehicles.

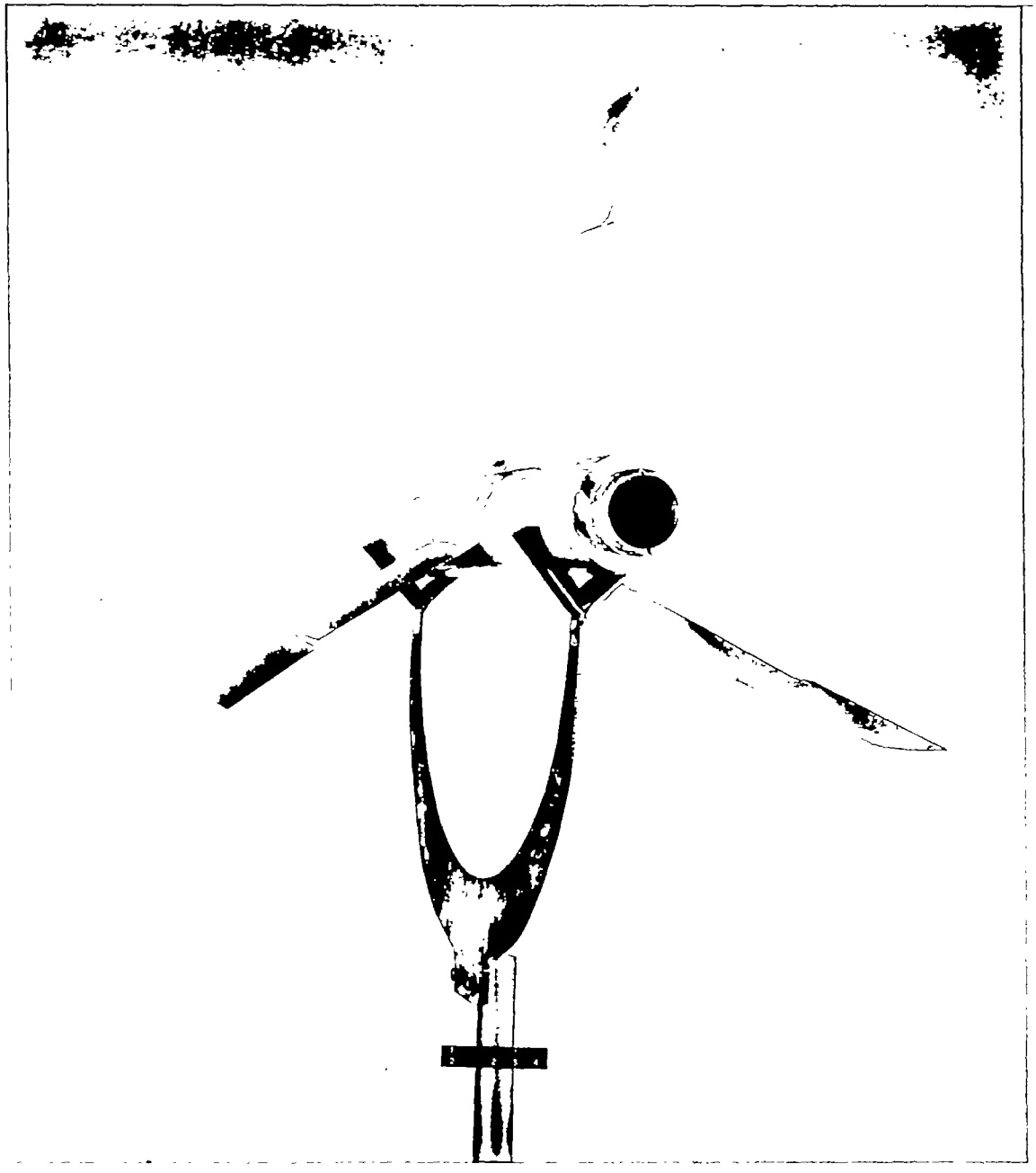

(b) Rear quarter view. Model 3. L-76461.1

Figure 3.- Continued.

[redacted]

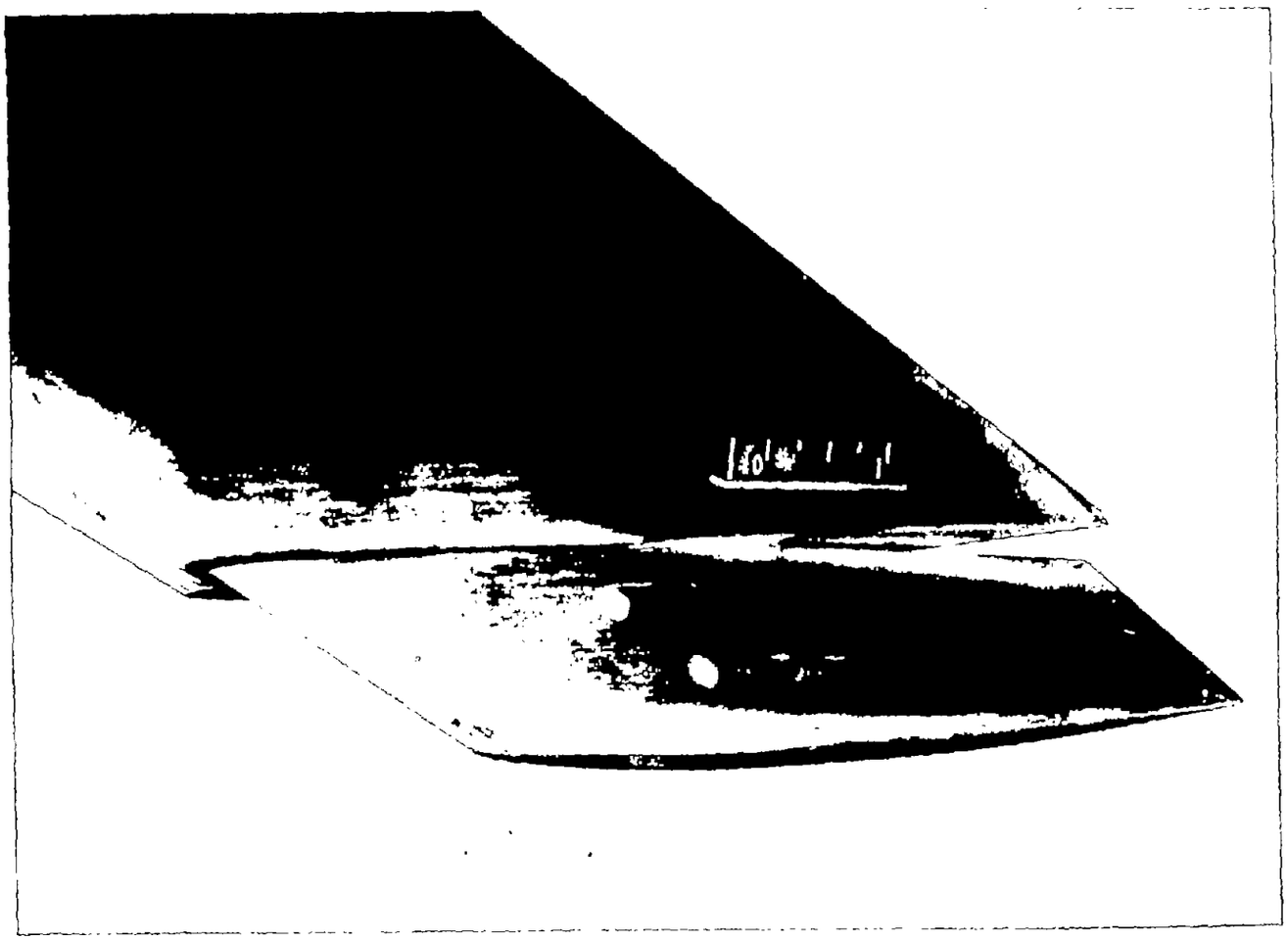

L-76463

(c) Detail showing rotated wing segment. Model 4.

Figure 3.- Concluded.

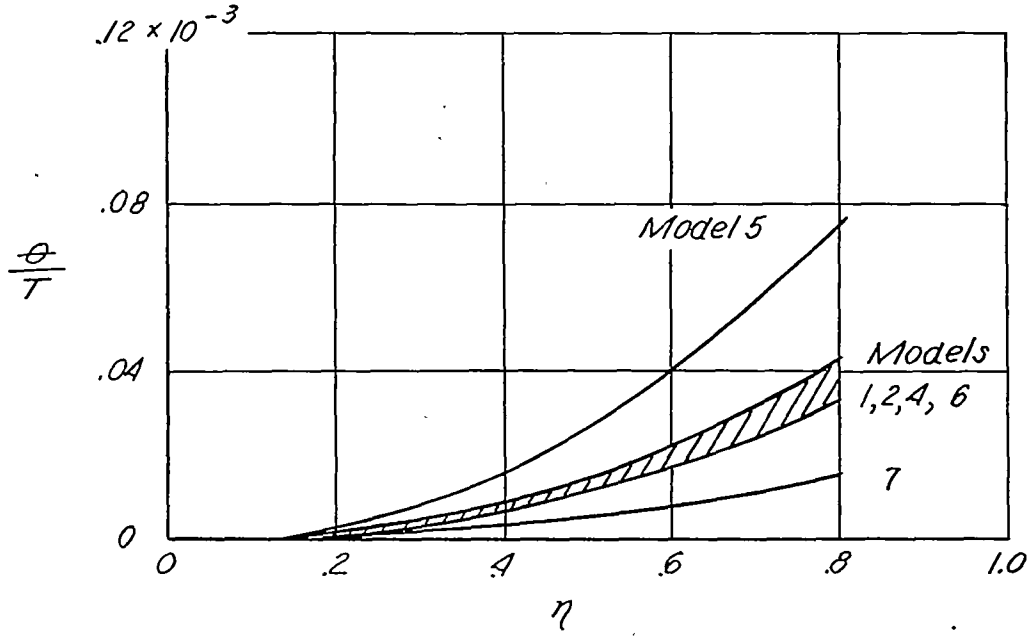

Figure 4.- Variation of the torsional stiffness parameter with span.

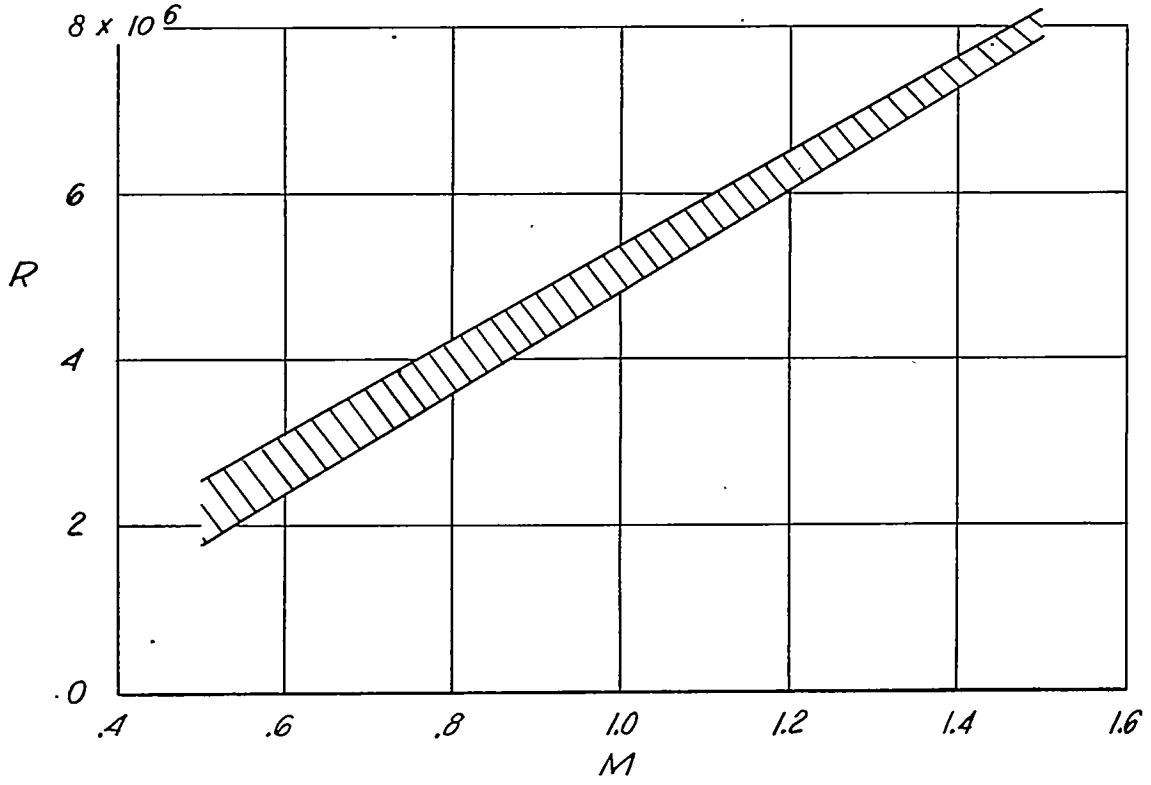

Figure 5.- Variation of test Reynolds number with Mach number. Reynolds number based on mean exposed chord (0.72 foot).

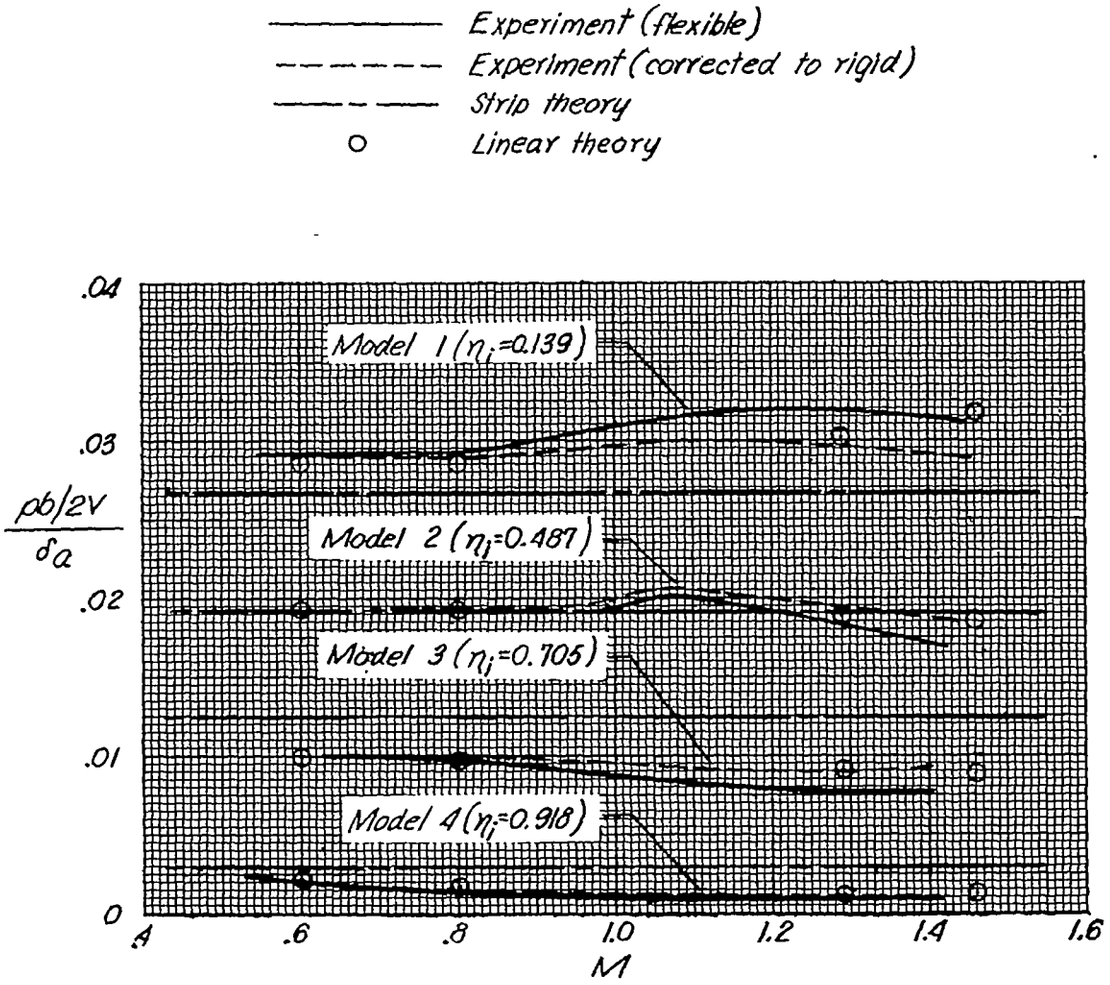

Figure 6.- Rolling effectiveness due to unit aileron deflection of full-exposed-span full-chord ailerons. $\Lambda = 45^{\circ}$; $\lambda = 0.6$; NACA 65A006 airfoil section.

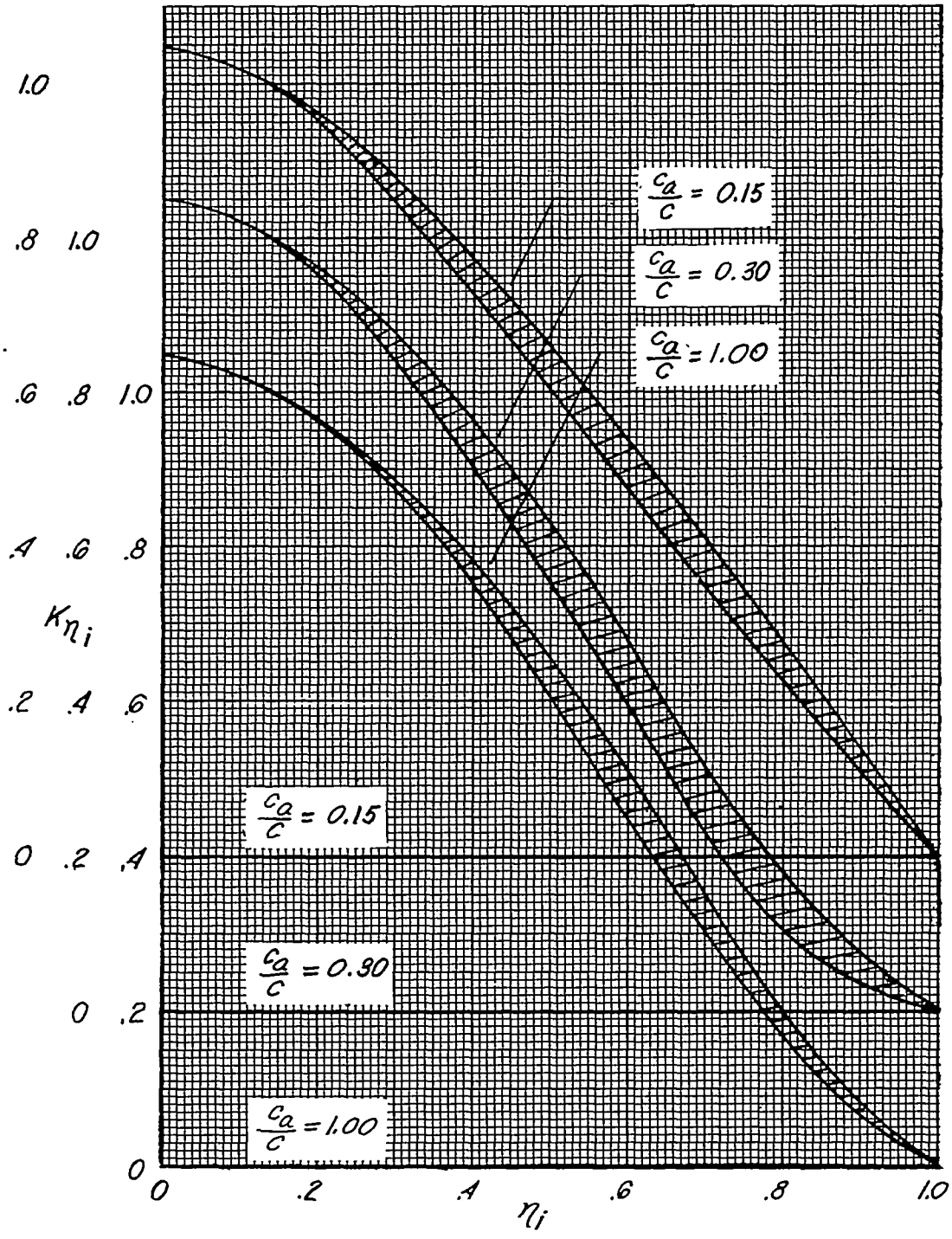

Figure 7.- Fraction of full-exposed-span rolling effectiveness retained by outboard partial-span ailerons. Envelope curves enclose total scatter experienced in the Mach number range $0.6 \leqq M \leqq 1.4$. NACA 65A006 airfoil section; $\Lambda = 45^{\circ}$; $\lambda = 0.6$; corrected to rigid wing values.

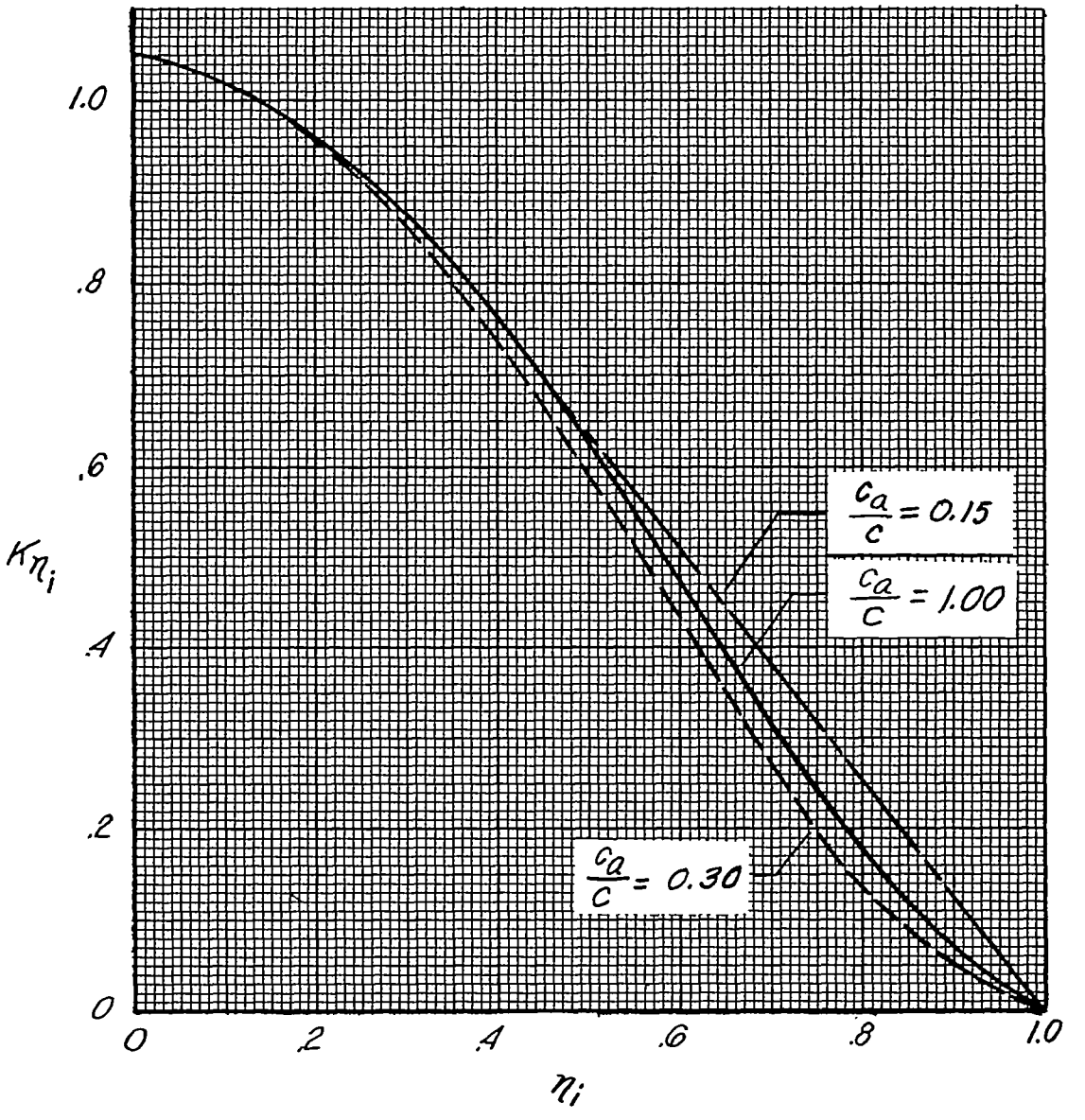

Figure 8.- Variation of rolling effectiveness with extent of aileron span for ailerons extending to the wing tip. $\Lambda = 45^{\circ}$; $\lambda = 0.6$; NACA 65A006 airfoil section; corrected to rigid wing values.

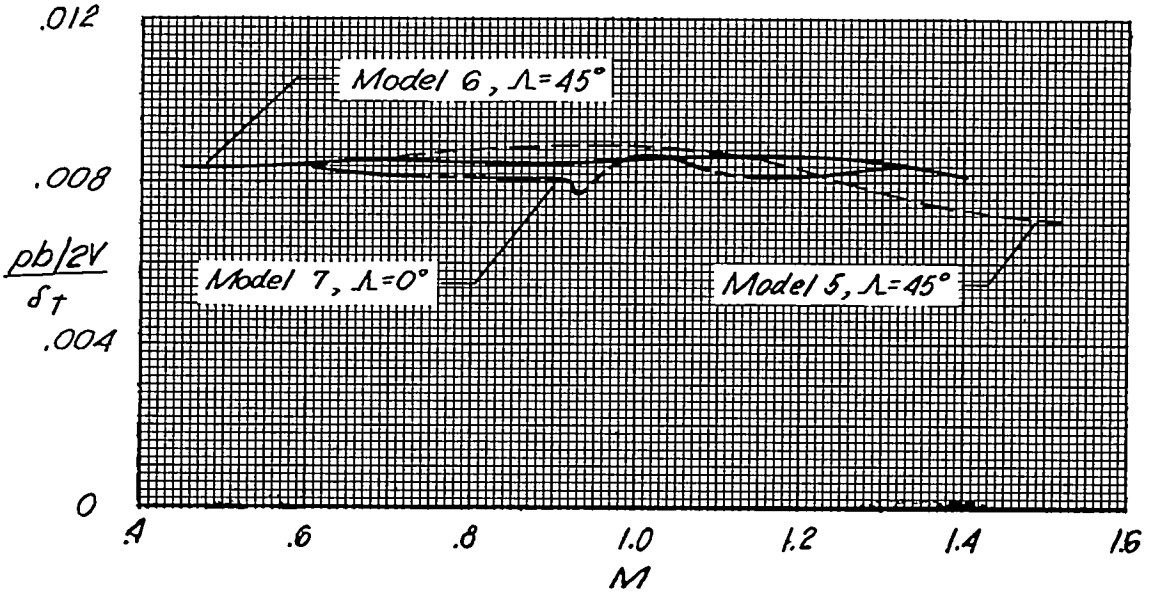

(a) Flexible.

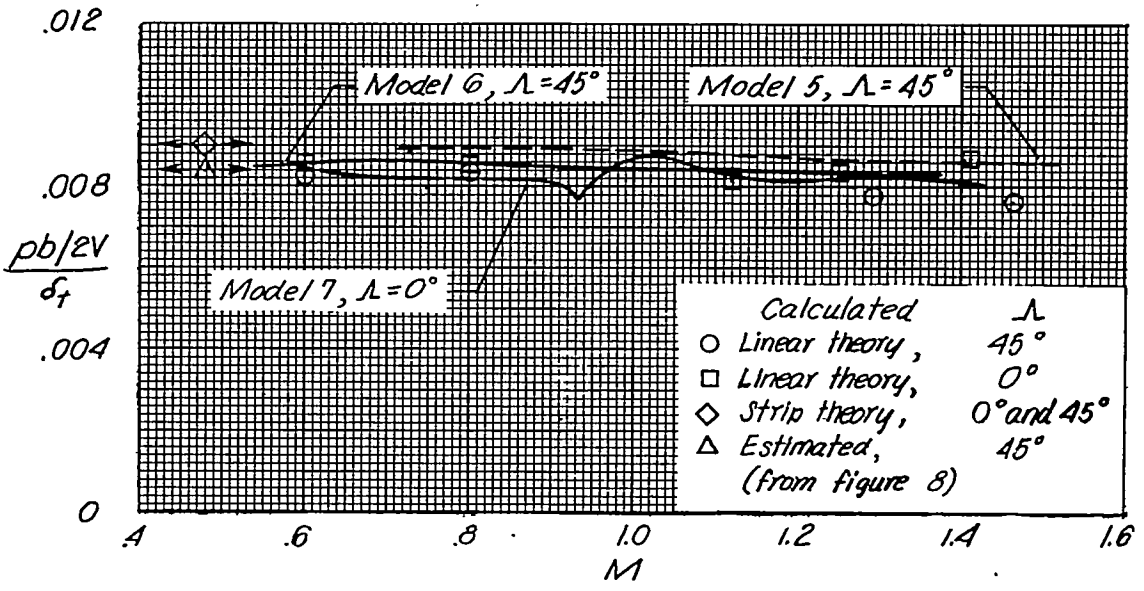

(b) Corrected to rigid.

Figure 9.- Comparison of rolling effectiveness resulting from cubic distribution of wing twist with several methods of estimation. $\Lambda = 0^{\circ}$ and 45°; $\lambda = 0.6$.

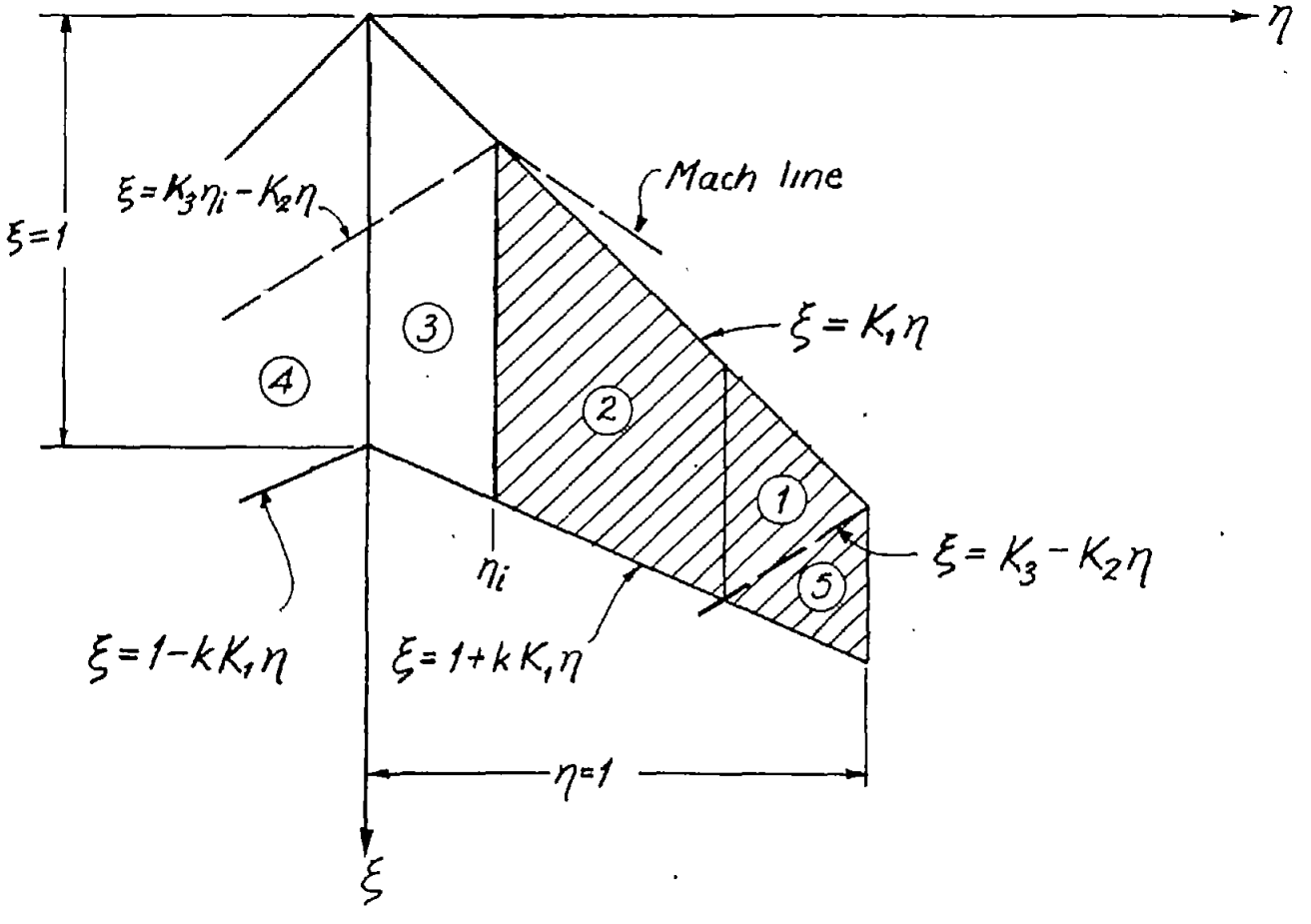

Figure 10.- Axis system and notation used in the calculations.

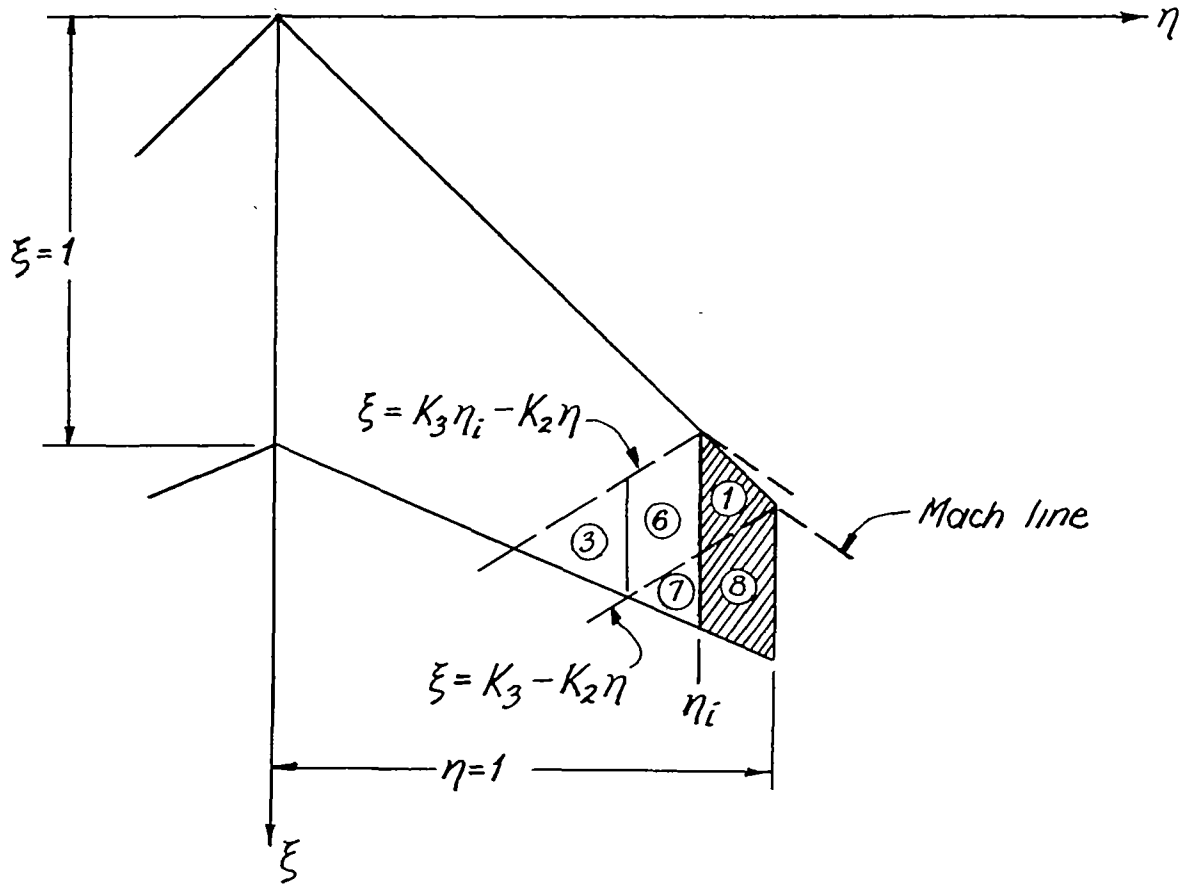

Figure 11.- Regions associated with model 4.

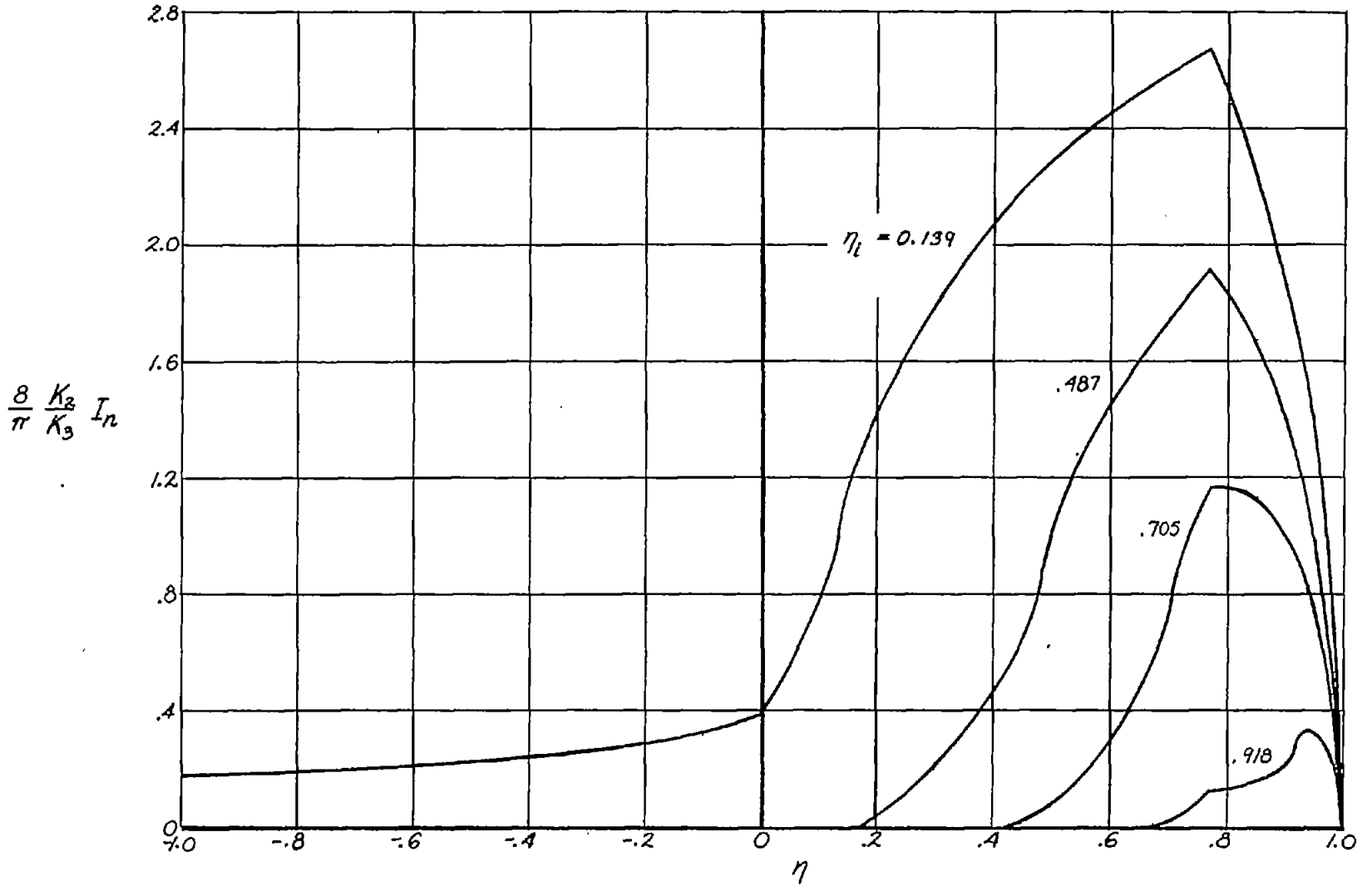

Figure 12.- Span load distribution for models tested. $\beta m = 0.765$.

NACA-Langley - 9-14-54 - 250